
3D seismic travel time surveying – a comparison of the time-term method and tomography (an example from an archaeological site)

J. Valenta*, J. Dohnal†

to appear in the Journal of Applied Geophysics, doi:10.1016/j.jappgeo.2007.04.002
available at: <http://www.sciencedirect.com/science/journal/09269851>

Abstract

The seismic tomography is an almost exclusive method in routine interpretation of 3D refraction datasets. However, the gradient model usually used for the tomography methods might not always be the most suitable one. In some cases, the layer-based model might be more appropriate. In this article, one simple layer-based approach is introduced, based on a modification of the time-term method. It enables computation of lateral velocity changes of a refractor in highly heterogeneous media. Applications and results of these two methods are then compared on the example of a seismic survey at a medieval castle. This case study proved that the time-term approach may yield results which surpass the tomography ones. However, a combination of the two methods is recommended.

1 Introduction

The 3D seismic prospection is still not very common in routine shallow seismic investigations. This fact can be ascribed to a number of reasons, one of which is the complexity of data processing. However, in the case of a highly heterogeneous environment, like at archaeological sites, the benefits of 3D prospection highly exceed the negatives. In this paper we report on the application of a modified time-term method to a 3D seismic prospection at the selected area of the Děvín medieval castle, and a comparison with the tomography method.

The most common technique in the processing of 3D refraction data sets is the traveltimes tomography. This method is based on the concept that the media, where the seismic waves propagate, have a velocity gradient. This implies the main drawback of tomography methods. If the geological environment is closer to the layered model than to the gradient one and layer boundaries are to be obtained, the gradient model might be problematic. Even if the algorithms combining the tomography and interface inversion do exist, their application is not without problems. The second disadvantage of the tomography methods is the complexity of raytracing in 3D media and the consequent very long computational times. The latter was overcome by introducing the back-projection method (Hole, 1992), where the time field is computed using the finite-difference algorithm and raytracing is performed backwards from the receiver to the source perpendicular to the isochrons of the time field. This raytracing is fast and stable as the appropriate raypath is always found.

The approach described by Hole et al. (1992) can be considered as an intermediate step between the tomography and interface inversion method. It employs 3D raytracing to obtain traveltimes.

*Institute of Rock Structure and Mechanics, Academy of Sciences of the Czech Republic, V Holešovičkách 41, 182 09 Prague 8, Czech Republic.

†Institute of Hydrogeology, Engineering Geology and Applied Geophysics, Faculty of Science, Charles University in Prague. Albertov 6, 128 43 Prague 2, Czech Republic.

Then, an estimate was utilised of the partial derivative relating the depth of the interface to the travelttime.

Another approach to the processing of 3D data sets is to simply fit layer boundaries into data, using the equation of head wave in the layered media. This is exactly what the time-term method does. It is only necessary to extend the original time-term method to enable also the computation of lateral changes of the velocity of the refractor, much like in the paper of Hear and Clayton (1986).

2 History, geological and geophysical settings

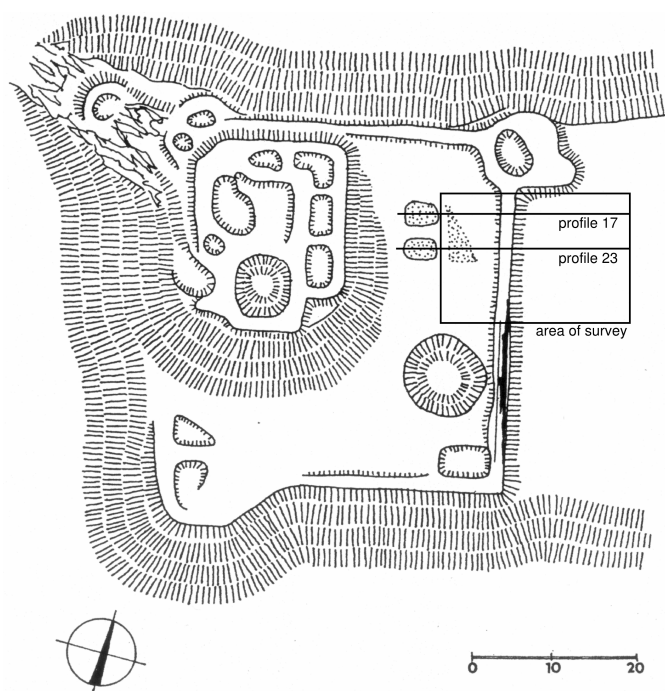


Figure 1: A map of remnants of the Dėvín Castle according to the archaeological propection (Durdik, 1999). Plotted is the area of geophysical research.

degree of weathering and usually ranges between 1000 and 4000 m/s (the latter for highly compact limestones). The micritic limestones on the locality might be expected to have velocities between 1700–3500 m/s.

The soil mantle this particular case have velocities ranging roughly between the 300 and 500 m/s, which are often encountered velocities for the soil mantle.

Velocities in walls are similar to velocities in bedrock, but not necessarily. Velocities in moat are hard to estimate. They depend on the filling of the moat.

3 Data acquisition

The part of the castle where relics of a rampart were apparent from the topography (fig. 1) was selected for the test survey. Shallow seismic refraction was selected, among other geophysical methods (DC tomography, gravity survey), to reveal remnants of the castle here. The gravity survey did not bring any useful information. The results of DC tomography were questionable,

The castle of Dėvín was a small 14th century fortification built on top of an elevation upon the Vltava River in the southern part of Prague. The castle was built some time before 1338 by Štěpán of Tetín. The castle was probably destroyed and abandoned during the Hussite wars in the first half of the 15th century. In the early 16th century, the remnants were used as a military target for testing guns. Even after this, the remnants were still apparent until the early 19th century when they were totally destroyed, probably exploited as building stones. Only parts of the castle are apparent in the present terrain morphology.

The geological bedrock is formed by Devonian limestones and micritic limestones, weathered on the top. Limestones are covered with Quaternary loess, the thickness of which does not exceed 1.5 m over the whole site.

Velocities of the highest parts of the bedrock are hard to estimate because they highly depend on the de-

probably due to the substantial electromagnetic disturbances from nearby railway. Therefore these methods will not be mentioned further.

Two 2D profiles were measured, crossing the assumed rampart, and a 3D seismic refraction was carried out in this area. Seismic data from both sources were processed by picking arrival times and computing the gradient and layered models. The gradient models were derived using the tomography technique. The 2D layered models were obtained using the plus-minus method (Hagedoorn, 1959). The 3D layered model was computed by a linear least-squares fitting of a refractor boundary to the data – a modification of the original time-term method. This method is described in Section 3.

The 2D profiles were 34.5 metres long, and were measured using a 1.5 metre distance between geophones. 3D data were obtained in a grid, where the geophones were deployed in a 4×4 metres mesh interlaced with the same mesh of sources, thus both together created a mesh of 2×2 metres. Moreover, additional shots were deployed on all four sides of the grid at a distance of five metres. In total, 24 geophones and 64 shots were used.

4 Processing of 3D data sets

4.1 Time-term method

The time-term method of seismic refraction is a simple method of refraction data analysis, in use since 1960. It was first described by Scheidegger and Willmore (1957). They used the equation for traveltime of the refracted wave on a dipping plane

$$t = \frac{HA \cos \theta}{V_1} + \frac{HB \cos \theta}{V_1} + \frac{\Delta \cos \phi}{V_2}, \quad (1)$$

where Δ is the distance between shotpoint A and receiver B , HA is a normal depth to the refractor at point A , HB is a normal depth to the refractor at point B , V_1 is the velocity of the top layer, V_2 is the velocity of the bottom layer, θ is the critical angle and ϕ is the dip of the refractor (see fig. 2). The $\cos \phi$ term is usually omitted as it is assumed that the dip is not steep and the term is roughly equal to 1. Then, for a set of traveltimes, we can build a system of linear equations which gives the depth to the refractor and the refractor velocity. This original method employs a constant refractor velocity.

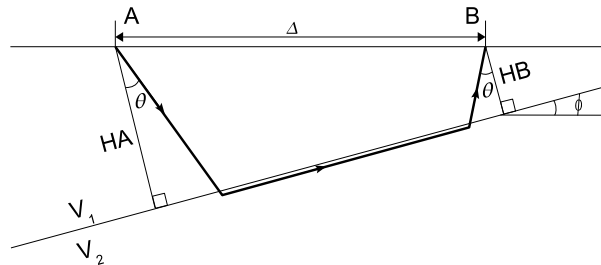


Figure 2: A ray path along a dipping refractor (after Scheidegger, Willmore, 1957).

We modified the method in a manner that it enabled a computation of lateral velocity changes along the refractor. This is similar to the method described by Hearn and Clayton (1986). However, we do not use the velocity depth profiles for station and event delays because this is not common in shallow seismics. Vertical velocity changes, if necessary, can be expressed by a higher number of layers. The lateral velocity changes of the overlying layer are determined from the direct wave. The solution of the obtained system of linear equations also differs from the solution described by Hearn and Clayton (1986). In order to stabilise the inversion process we introduced an a priori information to the equations and solved the system using the singular value decomposition. This is necessary for applying this method to such highly heterogeneous media.

We divide the refractor into $n \times m$ cells, each with a constant velocity. There are X, Y, Z coordinates of the p sources and q receivers. Now we have to find the ray path for each source–receiver pair along the refractor. The raytracing in three dimensions is generally a complex problem. To keep the computations simple we avoided raytracing by assuming straight raypaths, although we are aware of bringing an error into the dataset. The gain is the simplicity and

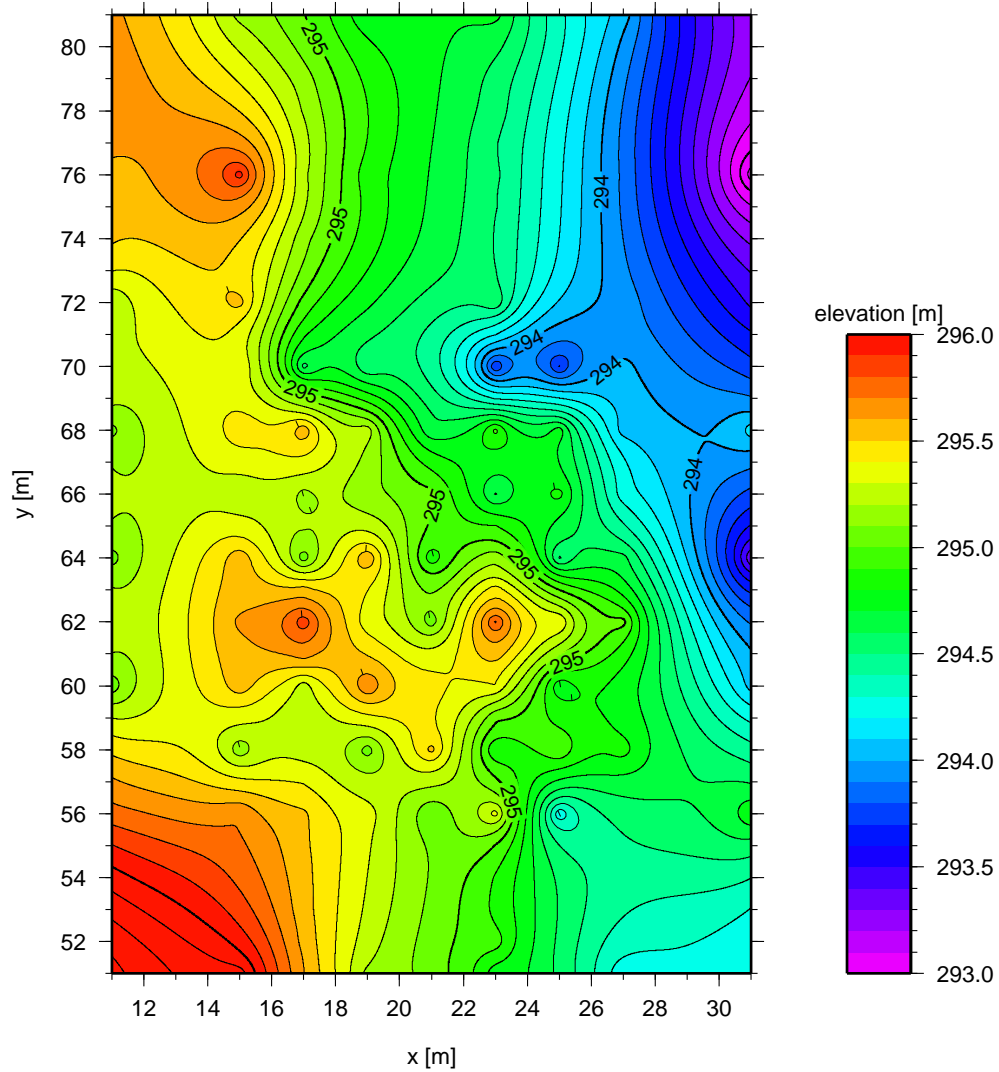


Figure 3: Time-term method – elevation of refracting boundary.

computational speed. The modified equation is then:

$$t_{ij} = \frac{HA_i \cos \theta_{Ai}}{V_{1Ai}} + \frac{HB_j \cos \theta_{Bj}}{V_{1Bj}} + \sum_{k=1}^m \sum_{l=1}^n \frac{\Delta_{kl}}{V_{2kl}}, \quad (2)$$

where t_{ij} is the travelt ime between i -th source and j -th receiver, HA_i is the depth beneath the i -th source, HB_j is the depth beneath the j -th receiver, θ_{Ai} , θ_{Bj} are the critical angles in the areas of i -th source or j -th receiver, respectively, V_{1Ai} , V_{1Bj} are velocities in the upper layer beneath the i -th source and j -th receiver, Δ_{kl} is the length of the ray path in the kl -th cell of the refractor and, finally, V_{2kl} is the velocity of the kl -th cell of the refractor. The velocities in the upper layer can be determined directly from the travelt ime curves. The velocities of the refractor cells and depths to the refractor beneath the sources and receivers are the unknowns.

We substituted slownesses s , the velocities reciprocals, for velocities V . Finally, for the whole dataset we obtained a system of $p \times q$ linear equations with $p + q + n \times m$ unknowns – depths H and slownesses of the refractor s . The system can be expressed in the form:

$$\mathbf{t} = \mathbf{A}\mathbf{x} \quad (3)$$

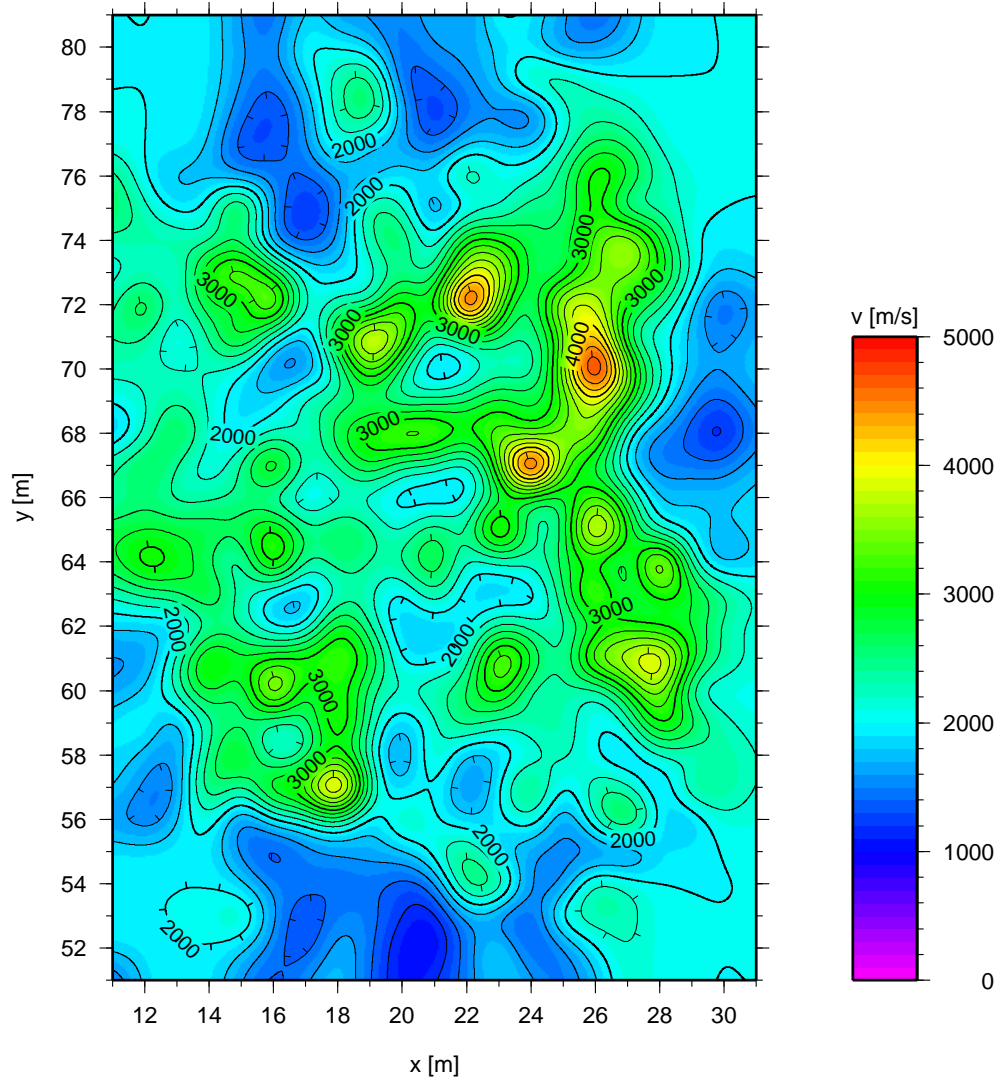


Figure 4: time-term method – refracting boundary velocities.

where \mathbf{t} is the column vector of measured traveltimes, \mathbf{x} is the vector of unknowns, and \mathbf{A} is the matrix of coefficients:

$$\mathbf{A} = \begin{pmatrix} \cos \theta_{A_1 s_{1A_1}} & 0 & \dots & 0 & \cos \theta_{B_1 s_{1B_1}} & 0 & \dots & 0 & \Delta_{11} s_{211} & \dots & \Delta_{mn} s_{2mn} \\ 0 & \cos \theta_{A_2 s_{1A_2}} & \dots & 0 & \cos \theta_{B_1 s_{1B_1}} & 0 & \dots & 0 & \Delta_{11} s_{211} & \dots & \Delta_{mn} s_{2mn} \\ 0 & 0 & \dots & \cos \theta_{A_p s_{1A_p}} & \cos \theta_{B_1 s_{1B_1}} & 0 & \dots & 0 & \Delta_{11} s_{211} & \dots & \Delta_{mn} s_{2mn} \\ \cos \theta_{A_1 s_{1A_1}} & 0 & \dots & 0 & 0 & \cos \theta_{B_2 s_{1B_2}} & \dots & 0 & \Delta_{11} s_{211} & \dots & \Delta_{mn} s_{2mn} \\ 0 & \cos \theta_{A_2 s_{1A_2}} & \dots & 0 & 0 & \cos \theta_{B_2 s_{1B_2}} & \dots & 0 & \Delta_{11} s_{211} & \dots & \Delta_{mn} s_{2mn} \\ \vdots & \vdots \\ 0 & 0 & \dots & \cos \theta_{A_p s_{1A_p}} & 0 & 0 & \dots & \cos \theta_{B_q s_{1B_q}} & \Delta_{11} s_{211} & \dots & \Delta_{mn} s_{2mn} \end{pmatrix} \quad (4)$$

Critical angle θ is in principal unknown, as we do not know the velocity of the underlying layer. This can be bypassed by assigning an a priori value of velocity to the refractor and solving the system. Then, the computed velocities can be used for the computation of θ in a low number of iterations.

Solution of this linear system gives directly searched depths and slownesses. However, this system is usually ill determined, and some kind of regularisation is necessary. Suitable approach to regularisation is to add an a priori information. This was well described by Tarantola (2005).

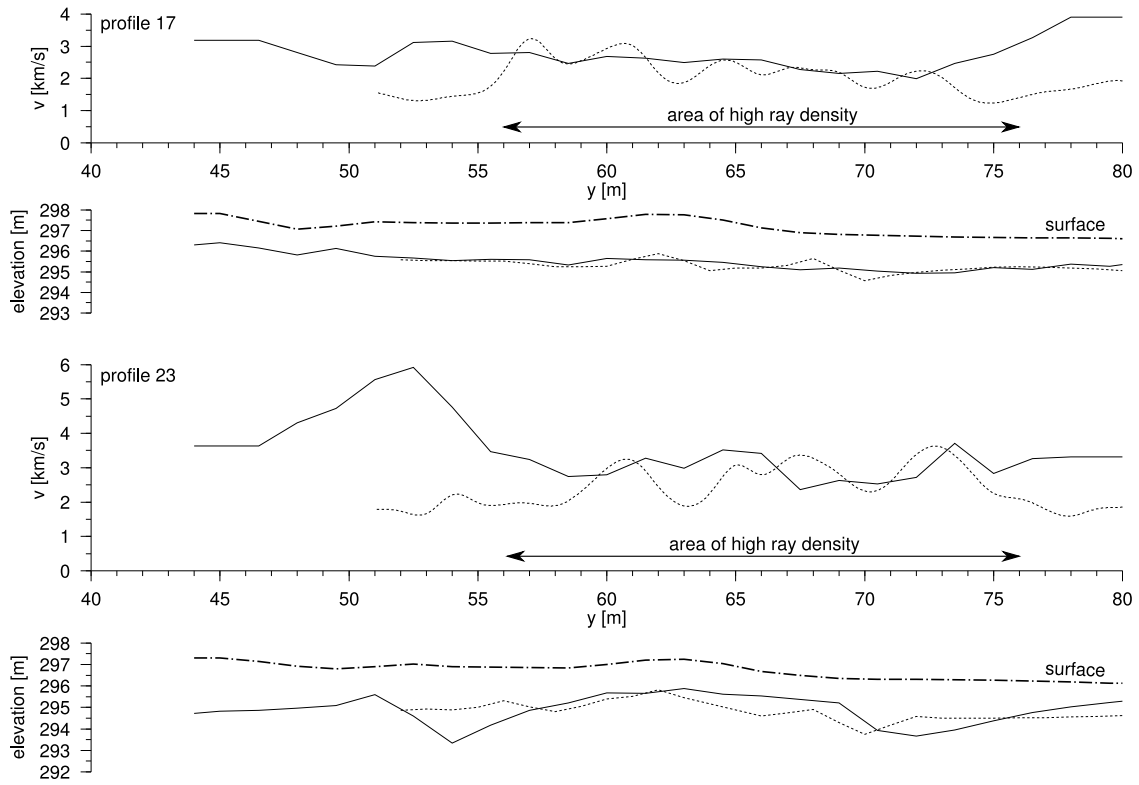


Figure 5: A comparison between the results of the time-term and plus-minus methods. The results of the plus-minus method are plotted in a solid line, time-term results in a broken line. A dotted line denotes the present surface. The plus-minus method was applied on a 2D measured profiles 17 and 23, the time-term method results are extracted from the gridded results of 3D survey. The depths have a good overall coincidence, the velocities coincide in the centre of the surveyed area, where the density of rays is the highest.

We added a vector of a priori information (depths under sources and receivers and slownesses of the refractor) \mathbf{m}_{pr}

$$\mathbf{m}_{pr} = (HA_{pr\ 1} \ \dots \ HA_{pr\ p} \ HB_{pr\ 1} \ \dots \ HB_{pr\ q} \ s_{2\ 11} \ \dots \ s_{2\ 1mn}), \quad (5)$$

covariance matrix of uncertainties σ_d of measured data \mathbf{C}_D :

$$\mathbf{C}_D = \begin{pmatrix} \sigma_d^2_{11} & 0 & \dots & 0 \\ 0 & \sigma_d^2_{12} & \dots & 0 \\ \vdots & \vdots & \vdots & \vdots \\ 0 & 0 & \dots & \sigma_d^2_{pq} \end{pmatrix} \quad (6)$$

and covariance matrix of uncertainties of a priori values \mathbf{C}_M , created in the same manner as the \mathbf{C}_D but with σ_{mpr} for every coefficient of vector \mathbf{m}_{pr} .

With a priori information, the system is (Tarantola, 2005):

$$\mathbf{x} = \mathbf{m}_{pr} + (\mathbf{A}^t \mathbf{C}_D^{-1} \mathbf{A} + \mathbf{C}_M^{-1})^{-1} \mathbf{A}^t \mathbf{C}_D^{-1} (\mathbf{t} - \mathbf{A} \mathbf{m}_{pr}), \quad (7)$$

where \mathbf{A}^t denotes transpose of matrix \mathbf{A} and \mathbf{A}^{-1} denotes inversion of matrix \mathbf{A} .

Solution of the equation, e.g., using the singular value decomposition method, gives the vector of unknowns \mathbf{x} . It is desirable to have an idea about how precisely resolved is each individual

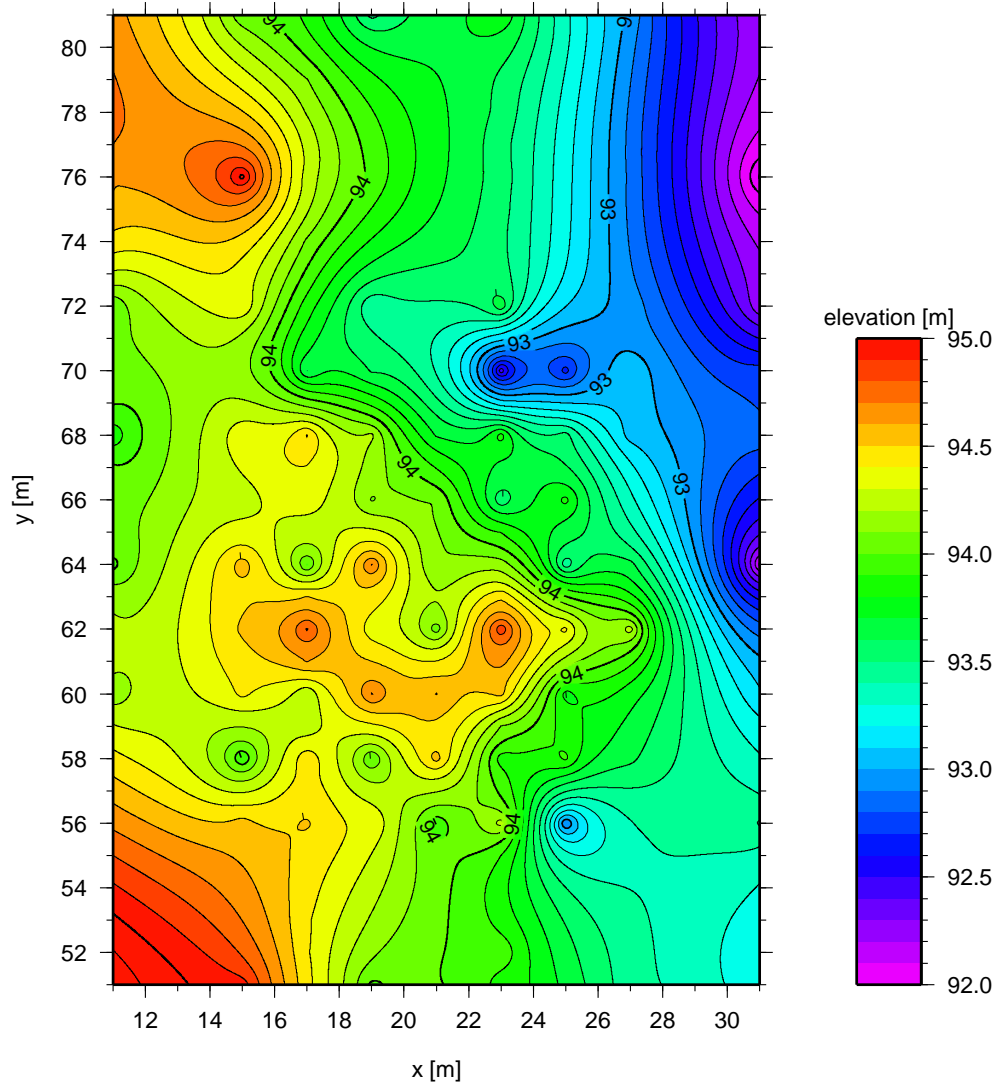


Figure 6: Time-term method – elevation of refracting boundary. A 10% error added to the data.

unknown. This can be achieved using the covariance operator $\tilde{\mathbf{C}}_{\mathbf{M}}$:

$$\tilde{\mathbf{C}}_{\mathbf{M}} = (\mathbf{A}^t \mathbf{C}_{\mathbf{D}}^{-1} \mathbf{A} + \mathbf{C}_{\mathbf{M}}^{-1})^{-1}. \quad (8)$$

Standard deviations σ of the resolved parameters are square roots of diagonal elements of the covariance operator $\tilde{\mathbf{C}}_{\mathbf{M}}$.

The only problem might be in supplying a priori information, but series of tests showed that the method is not too sensitive to slightly wrong parameters. Therefore, any values which give sense should be sufficient.

The described method can be easily extended to an arbitrary number of layers. The traveltimes equations will then contain two depth (thickness) elements (source and receiver) for each layer, and a matrix of refractor velocities for each boundary in the dataset. In a similar way it is also possible to extend it to a simultaneous use also of S-wave arrivals. The matrix of S-slownesses of each refractor will be appended. Depths for the S-wave boundaries may be the same as for the P-wave structure or different thereby increasing the number of unknown parameters, what should be more appropriate for particular geological settings.

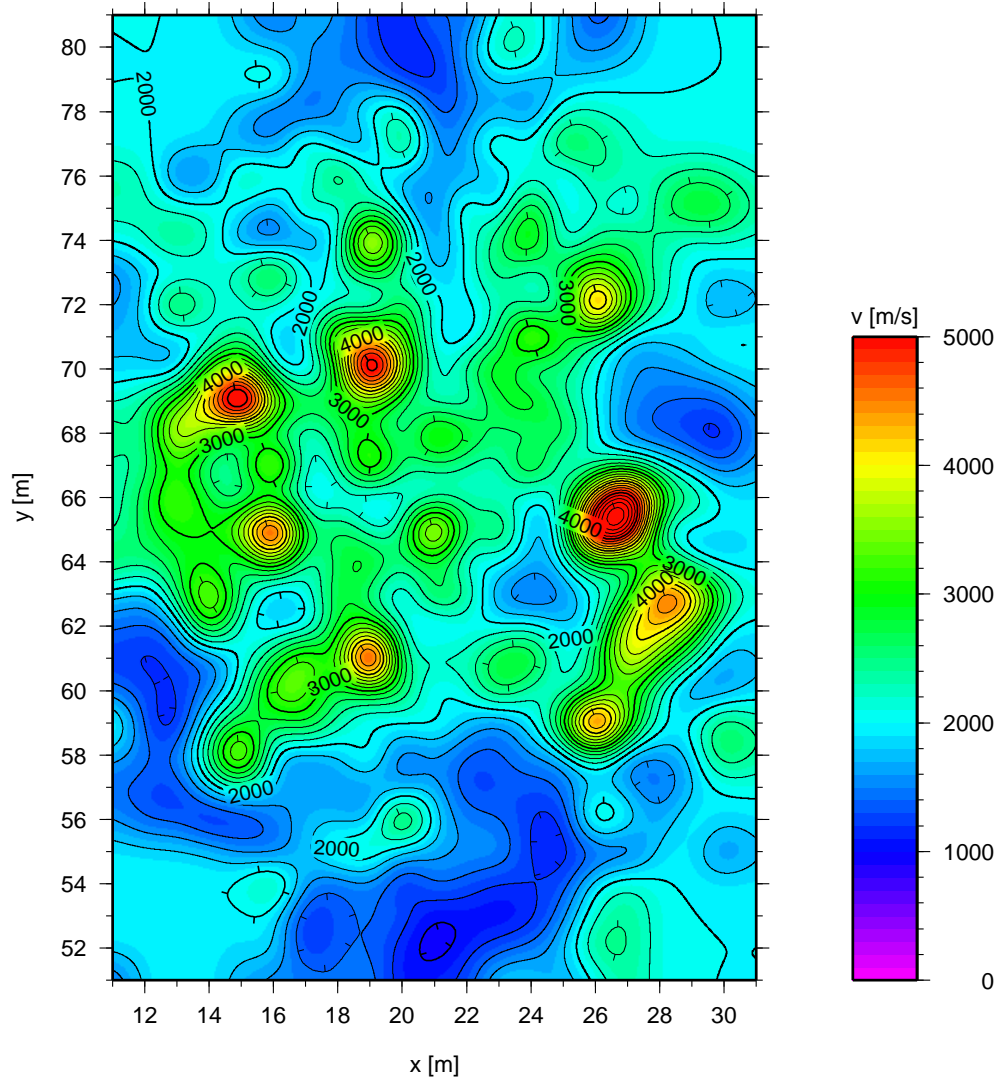


Figure 7: Time-term method – refracting boundary velocities. A 10% error added to the data.

The results of the time-term method are plotted in figures 3 and 4. Reliability of this method was tested by adding artificial noise to the data and by comparing computed results with those from the plus-minus method.

The first test was to compare results for the measured dataset and for the same dataset with a 10% error added to the traveltimes. This error is quite large, and such a noisy dataset would not be usually accepted as a reliable one. The results (figures 3, 4, 6, 7, 8, 9) show that the computed depths of the interface are affected to only a negligible degree. Velocities of the refracting boundary are affected to a higher degree, however, the main archaeological features are still apparent.

The depths are affected less than the velocities, because they are better determined in the equations (see the matrix of coefficients A in the equation (4)). The depth beneath every source is determined by all equations, where this source is used (similarly also the depth beneath receivers). In contrast, not every velocity cell may be sampled by sufficient number of rays. Therefore the noisy datasets (or sparse datasets) should need more velocity damping or larger size of velocity cells.

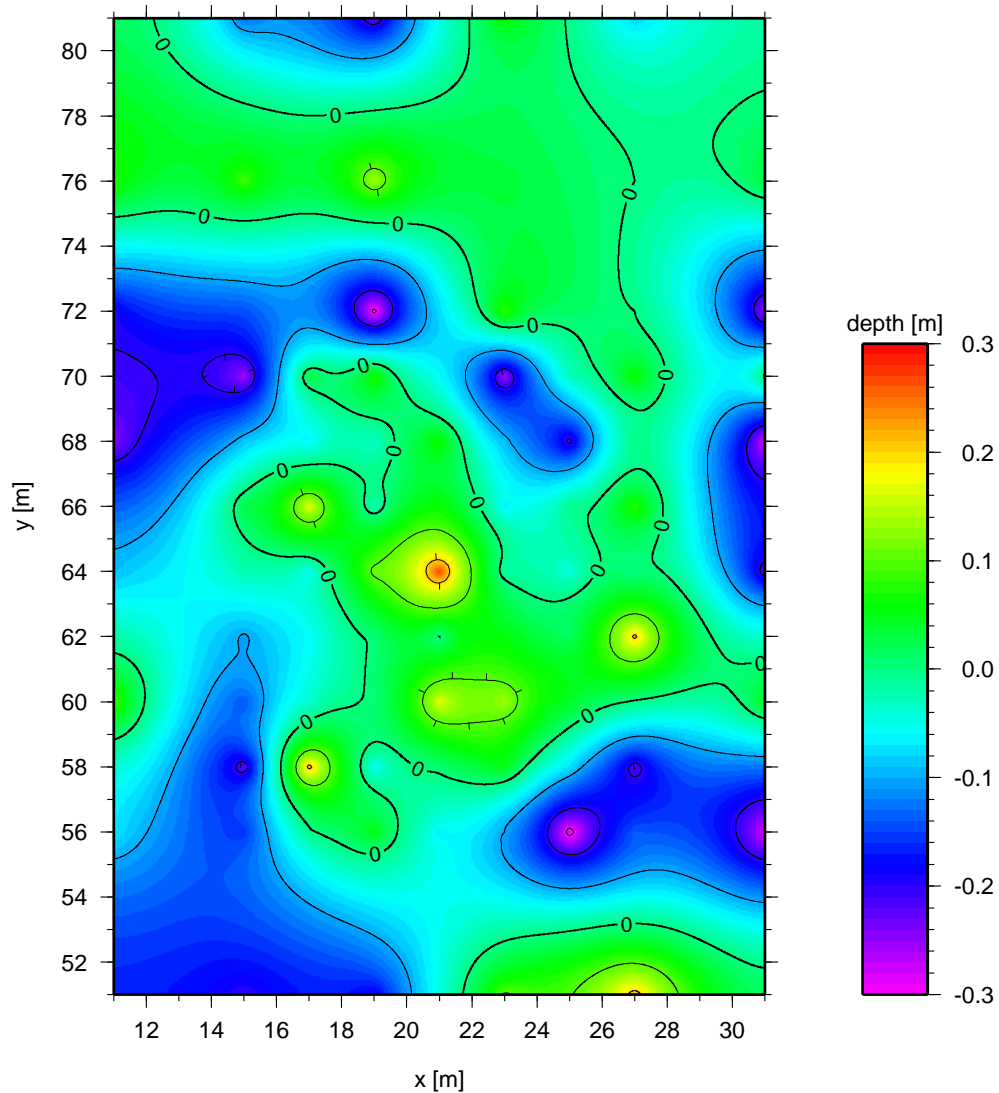


Figure 8: Time-term method – differences in the refractor depths for the original data and data with a 10% error.

4.2 Comparison of results of time-term and plus-minus methods

Results of 2D profiles and 3D time-term method are compared in figure 5. The depths to the interface show very good overall correlation with the exception that the time-term method's interface is less smooth. This is, among others, caused by the fact that the plus-minus method involves some amount of smoothing (the velocities of the refractor are computed using a moving window). This may or may not be the benefit of the time-term method. It can be considered beneficial in this case because the trace of a moat is visible also on profile 17, in contrast with the plus-minus method. The velocities reasonably correlate in areas where the ray coverage is sufficiently high – in the centre of the area.

Let us focus on the possible archaeological features resolved by these methods. An elevation of bedrock is visible at metres 62–63, where a possible rampart might be located. It is apparent on outputs from both methods, although very smoothed on profile 17 using the plus-minus method. The depression of bedrock around the metre 70 may be caused by a buried moat. It is well apparent on outputs from both methods on profile 23; however, it has a different shape. time-term results

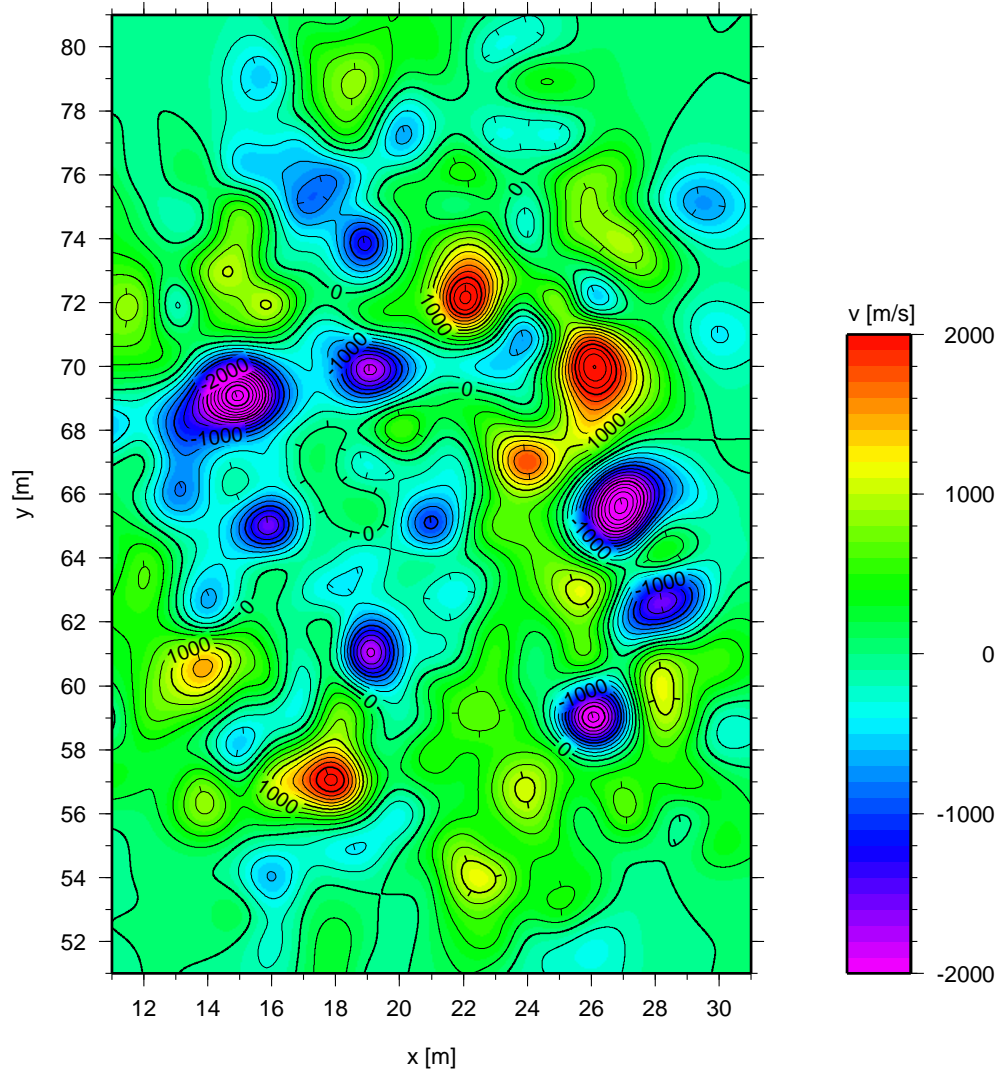


Figure 9: Time-term method – differences in the refractor velocities for the original data and data with a 10% error.

indicate only a hint of the moat on profile 17; however, this might be also caused by the fact that the moat is probably ending near this place. A large depression on profile 23 around the metre 54 and the corresponding high velocities visualised on the plus-minus method results seem to be an error. And finally, the data fit. The RMS errors for the plus-minus method are 1.444121 ms for profile 17 and 1.774981 ms for profile 23. The RMS error of the time-term method is 0.669905 for the whole dataset. The complete results of the time-term method are shown in figures 3, 4.

4.3 Tomography method

PStomo.eq algorithm by Ari Tryggvason was used for the seismic tomography (Tryggvason et al., 2002, Tryggvason, Linde, 2006). This program uses finite difference calculations for traveltimes and time field computations (Tryggvason, Bergman, 2006). The raytracing is performed “backwards” perpendicular to the isochrons of the time field (Hole, 1992). The advantage of this method is that an appropriate raypath is always found. The computations and subsequent raytracing are thus very stable. As no S-waves were measured in this case, the input for PStomo.eq consists

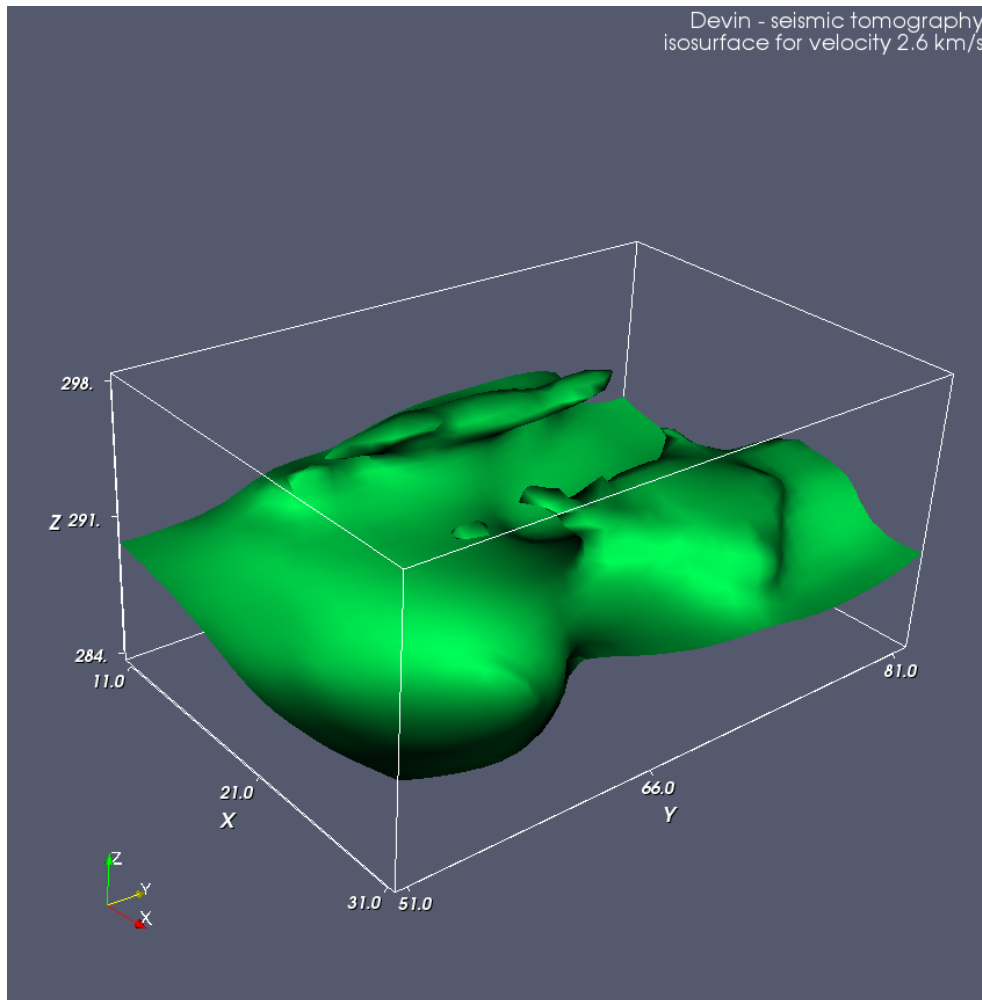


Figure 10: Seismic tomography – isosurface for the velocity of 2600 m/s.

only of P-wave arrival times. Smoothing during the inversion was kept as low as possible. Lower smoothing values were producing nonsensical (chaotic) models or even negative values of velocities. The results of travelttime tomography are shown in figures 10, 11. The RMS error of the travel time tomography is 0.930493 ms, while of the time-term method it is 0.669905 ms.

5 Archaeological interpretation

The interpreted ground-plan is based mainly on the time-term data processing because it gives a better resolution than the tomography method. For example, the interpreted walls are not clearly seen on the tomograms with the exception of the strengthened area at the gate. The moat, however, which is a larger structure, is visible also on the tomograms.

The tomograms, on the other hand, can be used for exploring the position of the castle on the former terrain. It seems that the castle was built on the small elevation and the ramparts stood on its edge. At the place where the ramparts were built, the elevation gain was about one metre and was further rising towards the centre of the castle. The moat was already outside this elevation. The position of this elevation was probably controlled by the presence of a more resistant, less weathered part of limestones.

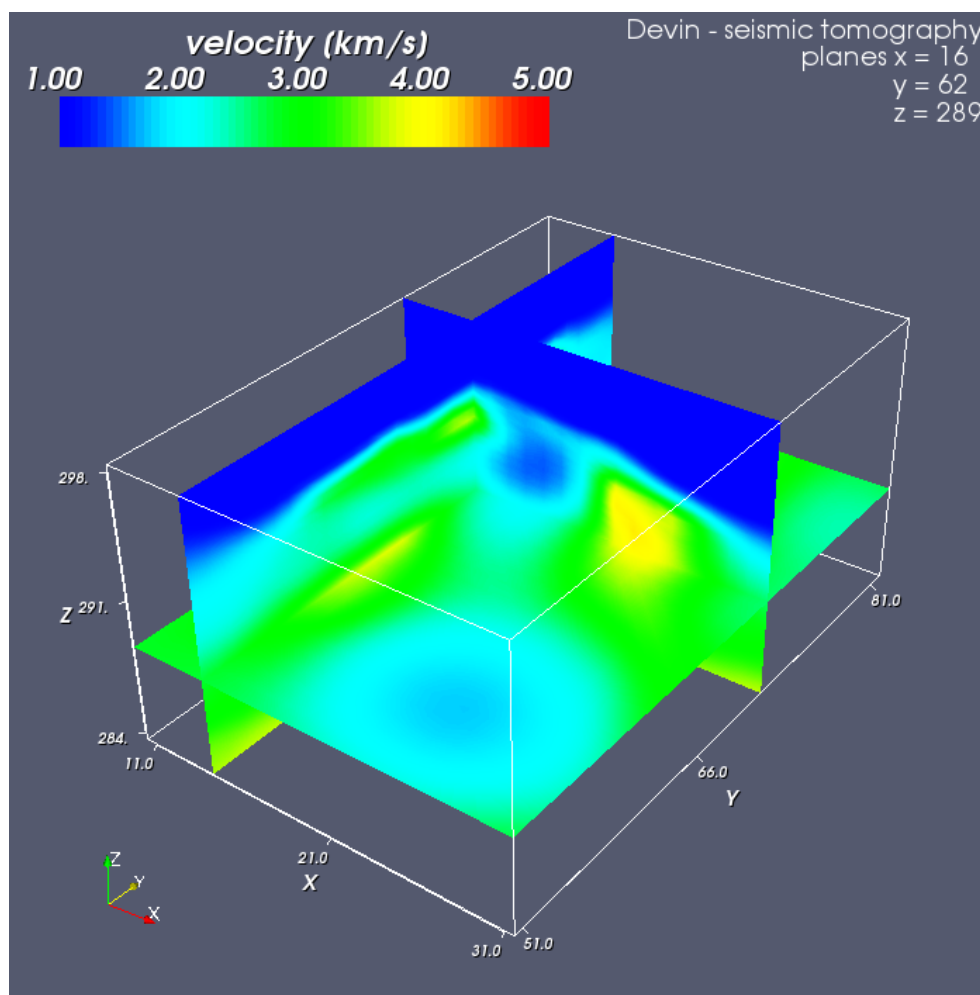


Figure 11: Seismic tomography – velocities in selected planes.

The interpreted ground plan of the castle and the cross-section are plotted on figures 12 and 13. Rests of the wall with a gate and a moat are visible. The moat is about six metres wide and, according to the tomography method, three metres deep. The velocities of seismic waves in the area of the moat are high (around 3000 m/s), and this may be caused by the fact that it is filled with relics of former ramparts. It is located 5 metres ahead of the castle walls. The moat seems to have ended near the x-coordinate of 16 m, probably due to the tower the remnants of which are visible to the north of the surveyed area.

The ramparts are expressed as an elevation of the refractor, and have higher velocities than their surroundings. They were two metres thick and further strengthened on both sides of the gate. The interpreted base of the ramparts lies two metres below the former surface. A depression in the refractor and a velocity decrease were observed in the area of the gate. This may be due to the pit used to further defend the gate.

6 Conclusions

It is no surprise that the 3D measurements give better results than the 2D ones, as can be seen from the presented results. To compare between the time-term (or other layered model-based

interpretation) and tomography (gradient model) methods is much more difficult. Pros and cons of these methods depend mainly on geological settings at each particular locality and on the type of model needed.

The tomography method usually seeks the smoothest possible model in order to stabilise the inversion process. This might be a limitation when we are looking for subtle structures, which is the case of archaeological prospection. On the other hand, it gives a better overview of larger structures where no details are desired.

The time-term method does not need any restrictions on smoothness of the model as the inversion process is linear. Therefore, even the subtle structures can be resolved, but the price is that the resulting values might oscillate and some amount of smoothing might then be necessary. Another benefit of the time-term method is its simplicity and speed. The results are computed on the order of minutes, compared to hours needed for tomography methods. The drawback is the necessity to assign individual travel times to corresponding layers.

The time-term method (or other layered-model method) should be chosen when the depth of the interface is to be resolved, because looking for interfaces in the tomography gradient model is not much precise. It also gives a better spatial resolution.

The tomography, in contrast, gives information about larger part of the “cube” below the measured area. The best option is to combine the two methods because they perfectly complement one another.

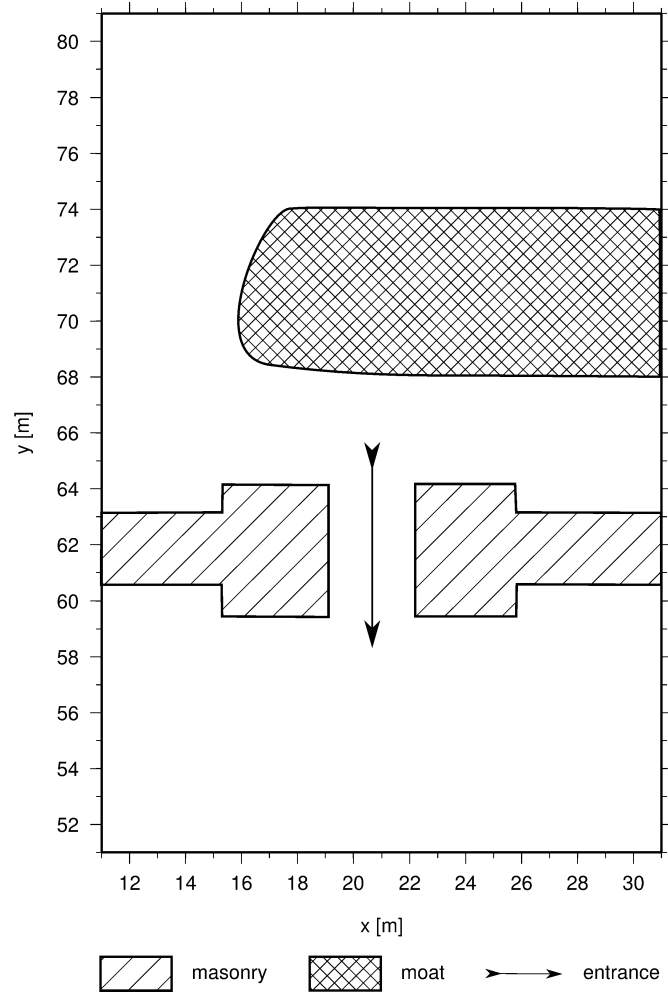


Figure 12: The interpretation of castle remnants based on all applied seismic methods.

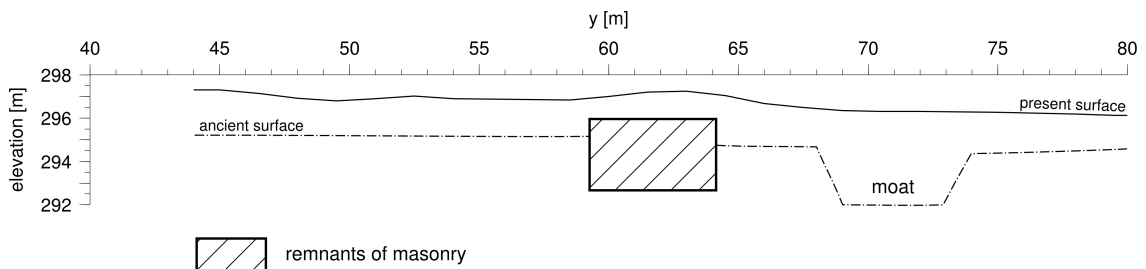


Figure 13: The interpreted cross-section along profile 23 based on all applied seismic methods. Plotted is the thickened base of a rampart at the side of the gate, a moat three metres deep and a possible surface from the time, when the castle was built. Note the small terrain elevation (about one metre) where the castle was built. This elevation is further rising to the centre of the castle.

Acknowledgements

This work was supported by the Ministry of Education of the Czech Republic, project No. MŠM 0021620855.

References

- Durdík, T., 1999. Ilustrovaná encyklopedie českých hradů. Libri, Prague, pp. 111–112 (in Czech).
- Hagedoorn, J. G., 1959. The plus-minus method of interpreting seismic refraction sections. *Geophysical Prospecting*, 7, 158–181.
- Hearn, T. M., Clayton, R. W., 1986. Lateral velocity variations in southern California. I. Results for the upper crust from Pg waves. *Bull. Seism. Soc. Am.*, 76, pp. 495–509.
- Hole, J. A., 1992. Nonlinear high-resolution three-dimensional seismic travel time tomography, *J. Geophys. Res.*, 97, pp. 6553–6562.
- Hole, J. A., Clowes, R. M., Ellis, R. M., 1992. Interface inversion using broadside seismic refraction data and three-dimensional travel time calculations, *J. Geophys. Res.*, 97, pp. 3417–3429.
- Scheidegger, A. E., Willmore, P. L., 1957. The use of a least squares method for the interpretation of data from seismic surveys, *Geophysics*, 22, pp. 9–21.
- Tarantola, A., 2005. *Inverse Problem Theory*. Society for Industrial and Applied Mathematics, Philadelphia.
- Tryggvason, A., Bergman, B., 2006. A travel time reciprocity inaccuracy in the time3d finite difference algorithm by Podvin & Lecomte, *Geophys. J. Int.*, 165, pp. 432–435.
- Tryggvason, A., Linde, N., 2006. Local earthquake (LE) tomography with joint inversion for P- and S-wave velocities using structural constraints, *Geophys. Res. Lett.*, 33, L07303.
- Tryggvason, A., Rögnvaldsson, S. Th., Flovenz, Ó. G., 2002. Three-dimensional imaging of the P- and S-wave velocity structure and earthquake locations beneath Southwest Iceland, *Geophys. J. Int.*, 151, pp. 848–866.